'Iolani Science Olympiad Pre-Nationals Practice

Division C

MATERIALS SCIENCE TEST

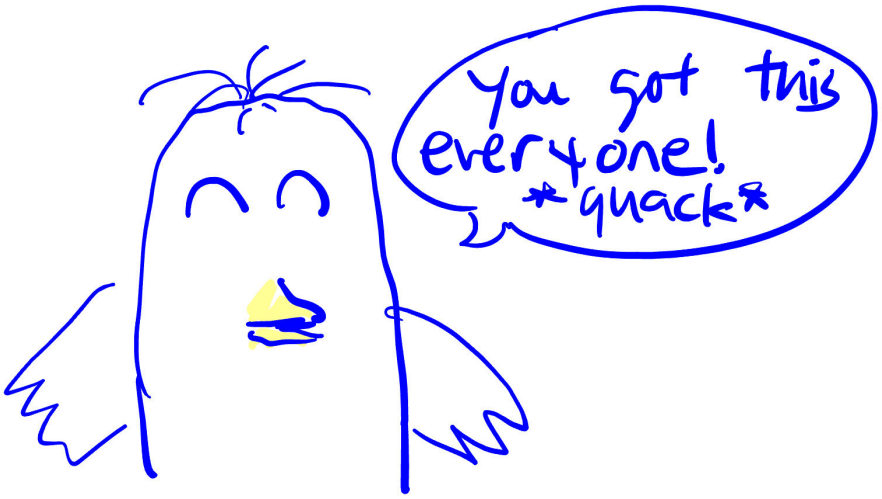

Name _____

Honolulu
2025

1 The Big Bad Multiple Choice Questions

1. In a face-centered cubic (FCC) lattice of ions, what fraction of the total lattice energy of the solid arises from interactions beyond the first coordination shell, assuming a point-charge model and using the Madelung constant?

(A) $\sim 5\%$

(B) $\sim 15\%$

(C) $\sim 30\%$

(D) $\sim 50\%$

2. Which of the following Bravais lattices cannot produce a powder X-ray diffraction pattern with systematically absent reflections of the form $h + k + l = \text{odd}$?

(A) Body-centered cubic (BCC)

(B) Face-centered cubic (FCC)

(C) Simple cubic (SC)

(D) Hexagonal close-packed (HCP)

3. The theoretical maximum packing efficiency of the hexagonal close-packed structure is:

(A) 68.0%

(B) 74.0%

(C) 52.4%

(D) 80.0%

4. In the rock-salt (NaCl) structure, the radius of the largest octahedral void (in units of the host sphere radius R) is:

(A) $0.155\,R$

(B) $0.414\,R$

(C) $0.732\,R$

(D) $1.000\,R$

5. Which of these oxide glass formers exhibits the highest glass transition temperature (T_g)?

(A) SiO_2

(B) B_2O_3

(C) P_2O_5

(D) GeO_2

6. In silicate glasses, increasing the fraction of modifier cations (e.g. Na^+) primarily:

(A) Increases network connectivity and raises T_g

(B) Breaks Si–O–Si linkages and lowers T_g

(C) Converts bridging oxygens to non-bridging oxygens but raises density

(D) Has negligible effect on optical refractive index

7. According to Zachariasen's rules for glass formation, which is *not* one of the rules?

(A) Oxygen atoms are linked to no more than two glass-forming atoms.

(B) Each glass-forming atom must be surrounded by a coordination number of at least three.

(C) Polyhedra share corners, not edges or faces.

(D) A random three-dimensional network is formed.

8. The so-called "fragility" of a glass-forming liquid describes:

(A) The steepness of the viscosity vs. temperature plot at T_g

(B) The susceptibility of the glass to mechanical fracture

(C) The amount of non-bridging oxygens in the network

(D) The difference between T_g and crystallization temperature T_x

9. Phase separation in alkali silicate glasses upon cooling is often a result of:

(A) Immiscibility between silica-rich and alkali-rich regions

(B) Crystallization of quartz nuclei

(C) Spinodal decomposition of polymer chains

(D) Diffusion-limited aggregation of modifier ions

10. Which pair of elements would exhibit the greatest degree of covalent character according to Pauling's scale of electronegativity?

(A) Na–Cl

(B) Si–O

(C) Mg–F

(D) Al–N

11. The Born exponent n in the Born–Mayer potential is most directly related to:

(A) The compressibility of the crystal

(B) The ionic radii ratio

(C) The polarizability of the anion

(D) The bond dissociation energy at zero separation

12. Which of the following materials would you expect to have the highest cohesive energy?

(A) Metallic sodium

(B) Diamond (carbon)

(C) Ionic sodium chloride

(D) Amorphous silica glass

13. The work function of a metal is primarily governed by:

(A) Van der Waals forces between atoms

(B) Ionization energy of the isolated atom

(C) Strength of metallic bonding and electron density at the surface

(D) Electron affinity of the metal atom

14. Madelung's constant for the wurtzite (hexagonal ZnS) lattice is about 1.64. Which of these statements follows?

(A) The lattice energy of ZnS is lower than that of NaCl (Madelung ≈ 1.747) for the same interionic distance.

(B) ZnS must be metallic, not ionic.

(C) The coordination number in wurtzite is greater than in rock salt.

(D) Electrostatic energy is independent of Madelung constant.

15. The minimum radius ratio $r_{\text{cation}}/r_{\text{anion}}$ required for a cation to occupy a tetrahedral site in an anion lattice is approximately:

(A) 0.155

(B) 0.225

(C) 0.414

(D) 0.732

16. A compound with $r_{\text{cat}}/r_{\text{an}} \approx 0.732$ is most likely to adopt which coordination geometry?

(A) Linear (CN = 2)

(B) Tetrahedral (CN = 4)

(C) Octahedral (CN = 6)

(D) Cubic (CN = 8)

17. Which of these Laves phases (AB_2) is favored when $r_A/r_B \approx 1.225$?

(A) $MgCu_2$ (C15, cubic)

(B) $MgZn_2$ (C14, hexagonal)

(C) $MgNi_2$ (C36, hexagonal)

(D) Any of the above; Laves phases are insensitive to radius ratios

18. In a mixed halide perovskite, if the average anion radius increases by 10%, the perovskite tolerance factor t will:

(A) Increase by $\sim 10\%$

(B) Decrease by $\sim 5\%$

(C) Stay constant

(D) Increase, but by less than 10%

19. For alkali halides, the transition from the rock-salt to the wurtzite/ZnS structure occurs when $r_{\text{cat}}/r_{\text{an}} \lesssim 0.414$. Which of these should therefore show a wurtzite-type structure under ambient conditions?

(A) LiF ($r^+ = 0.76\,\text{Å}$; $r^- = 1.33\,\text{Å}$)

(B) NaCl ($r^+ = 1.02\,\text{Å}$; $r^- = 1.81\,\text{Å}$)

(C) KBr ($r^+ = 1.38\,\text{Å}$; $r^- = 1.96\,\text{Å}$)

(D) CsI ($r^+ = 1.67\,\text{Å}$; $r^- = 2.20\,\text{Å}$)

20. The energy of a small-angle tilt boundary varies approximately as:

$$\gamma \propto G b\,\theta$$

where G is the shear modulus, b the Burgers vector, and θ the misorientation angle (in radians). This relationship holds for θ up to about:

(A) 1°

(B) 5°

(C) 10°

(D) 15°

21. A $\Sigma 3$ coincidence-site lattice (CSL) boundary in a cubic metal corresponds to a misorientation of:

(A) 36.9° about $\langle 110 \rangle$

(B) 60° about $\langle 111 \rangle$

(C) 38.9° about $\langle 111 \rangle$

(D) 43.3° about $\langle 100 \rangle$

22. Which mechanism predominantly lowers the energy of a high-angle grain boundary upon annealing?

(A) Boundary migration reducing total boundary area

(B) Vacancy diffusion within the boundary core

(C) Precipitate pinning at the boundary

(D) Grain rotation without migration

23. Which imperfection introduces tensile stress fields in the surrounding lattice?

(A) Interstitial atom

(B) Vacancy

(C) Edge dislocation extra half-plane

(D) Screw dislocation

24. If the vacancy formation energy doubles, at the same temperature the equilibrium concentration of vacancies:

(A) Doubles

(B) Halves

(C) Squares

(D) Becomes its own square root

25. In a metal at 0.5 T_m (half melting temperature), the vacancy concentration is 10^{-4}. At 0.6 T_m, roughly what is the concentration, assuming constant vacancy formation energy?

(A) 10^{-6}

(B) 10^{-5}

(C) 10^{-3}

(D) 10^{-2}

26. For a cation of radius ratio $r_c/r_a = 0.30$ in an anion FCC lattice, the preferred site is:

(A) Tetrahedral

(B) Octahedral

(C) Cubic

(D) None (unstable)

27. Segregation of impurity atoms to grain boundaries lowers the boundary energy because of:

(A) Reduction of lattice parameter mismatch

(B) Elastic interaction between solute and boundary

(C) Increased boundary mobility

(D) Precipitation strengthening

28. A typical Frenkel defect in AgCl involves:

(A) Cl vacancy + Cl interstitial

(B) Ag vacancy + Ag interstitial

(C) Cl vacancy + Ag interstitial

(D) Ag vacancy + Cl interstitial

29. In an ideal Schottky defect in NaCl, the ratio of vacancies is:

(A) 1 Na^+ : 1 Cl^-

(B) 2 Na^+ : 1 Cl^-

(C) 1 Na^+ : 2 Cl^-

(D) 2 Na^+ : 2 Cl^-

30. The activation energy for self-diffusion in ionic crystals often includes both migration and formation energies. If $E_m = 0.5$ eV and $E_f = 1.0$ eV, the diffusion activation is:

(A) 0.5 eV

(B) 1.0 eV

(C) 1.5 eV

(D) 2.0 eV

31. The Burgers vector **b** of a perfect dislocation in a BCC metal is:

(A) $a\langle 100\rangle$

(B) $\frac{a}{2}\langle 111\rangle$

(C) $a\langle 110\rangle$

(D) $\frac{a}{2}\langle 110\rangle$

32. A mixed dislocation with edge and screw character lies at a tilt grain boundary. The edge component drives:

(A) Boundary climb

(B) Boundary migration

(C) Dislocation cross-slip

(D) Twinning

33. Which compound is least likely to exhibit Frenkel disorder?

(A) AgBr

(B) ZnS

(C) NaCl

(D) CsI

34. The equilibrium Schottky defect concentration in MgO (one Mg^{2+} + one O^{2-}) varies as:

$$C_s \propto \exp\left(-\frac{E_f}{2kT}\right).$$

The factor 1/2 arises because:

(A) Two ions removed per defect pair

(B) Charge neutrality constraint

(C) Migration barrier halved

(D) Vacancy formation enthalpy split

35. In olivine-type Mg_2SiO_4, the minor Fe^{2+} occupies:

(A) Octahedral M1 only

(B) Octahedral M2 only

(C) Both M1 and M2

(D) Tetrahedral sites

36. The effect of hydrostatic pressure on vacancy formation energy is to:

(A) Increase if defect volume positive

(B) Decrease if defect volume positive

(C) No change

(D) Reverse defect type

37. The Debye-Waller factor in diffraction includes contribution from point defects via:

(A) Static displacements only

(B) Thermal vibrations only

(C) Both static and thermal

(D) Neither

38. The Read–Shockley model fails for angles above:

(A) 5°

(B) 15°

(C) 30°

(D) 45°

39. Substitutional impurity diffusion in fcc metals occurs via:

(A) Direct interstitial jumps

(B) Vacancy mechanism

(C) Interstitialcy mechanism

(D) Grain boundary only

40. The concentration ratio of Frenkel defects in AgCl at equilibrium is:

$$\frac{n_{\text{vac}}}{n_{\text{int}}} = ?$$

Assuming equal formation energy for vacancy and interstitial, the ratio is:

(A) 1

(B) 2

(C) Depends on site multiplicity

(D) Zero

41. In UO_2, Schottky defects form more readily than Frenkel because:

(A) U^{4+} large cation

(B) O^{2-} small anion

(C) Charge vs. size considerations

(D) High oxygen mobility

42. Dislocation climb rate is controlled by:

(A) Vacancy diffusion

(B) Interstitial diffusion

(C) Glide plane friction

(D) Peierls barrier

43. The Kirkendall effect demonstrates:

(A) Vacancy flow markers
(B) Dislocation motion
(C) Grain boundary migration
(D) Precipitate growth

44. In semiconductor doped Si, vacancy concentration under n-type doping:

(A) Increases
(B) Decreases
(C) Unchanged
(D) Oscillates

45. Hydrogen in metals occupies:

(A) Octahedral only
(B) Tetrahedral only
(C) Both depending on T
(D) Substitutional only

46. Diffusion along grain boundaries is typically:

(A) Slower than lattice
(B) Same as lattice
(C) Faster than lattice
(D) Zero

47. The Cottrell atmosphere forms around:

(A) Grain boundaries
(B) Dislocations
(C) Twin boundaries
(D) Dr. Cottrell's office

48. Which defect pair conserves both mass and charge?

(A) Frenkel
(B) Schottky
(C) Both
(D) Neither

49. At the invariant eutectic point in the Cu–Sn system (227 °C), how many phases coexist?

(A) One
(B) Two

(C) Three

(D) Four

50. In the Fe–Fe_3C phase diagram, the eutectoid transformation at 727 °C is:

$$\gamma \;\rightarrow\; \alpha + \mathrm{Fe_3C}.$$

This reaction is classified as:

(A) Eutectic

(B) Eutectoid

(C) Peritectic

(D) Peritectoid

51. A peritectic reaction in a binary system is of the form:

$$L + \alpha \;\rightarrow\; \beta.$$

Which of the following is a peritectic system?

(A) Cu–Ni (complete solid solution)

(B) Pb–Sn (eutectic)

(C) Fe–C (eutectoid)

(D) Cd–Mg (peritectic)

52. The degree of freedom F at an invariant point in a binary isobaric phase diagram is given by Gibbs phase rule. At a eutectic ($P = 3$, $C = 2$), $F =$

(A) 0

(B) 1

(C) 2

(D) 3

53. In a monotectic reaction ($L_1 \rightarrow L_2 + \alpha$), the phase that exsolves is:

(A) α

(B) L_1

(C) L_2

(D) Alloys do not show monotectics

54. A congruently melting intermetallic forms a straight vertical liquidus line. Which of these compounds is congruent?

(A) Au–Cu_3

(B) Zn–Mg_2

(C) Ni–Al (NiAl)

(D) Ag–Cd

55. For a binary isomorphous system, the solidus and liquidus lines coincide at:

(A) Pure A and pure B only

(B) Eutectic composition

(C) Peritectic composition

(D) Every composition

56. Inside a miscibility gap, the limit of phase separation is defined by the spinodal curve where:

$$\frac{\partial^2 G}{\partial x^2} = 0.$$

Between the binodal and spinodal lines, decomposition occurs by:

(A) Spinodal decomposition

(B) Nucleation and growth

(C) Martensitic shear

(D) Diffusionless transformation

57. In a ternary phase diagram at a fixed temperature, the tie-triangle connects three phases α, β, γ. The overall alloy composition lies inside this triangle; phase fractions are given by:

(A) Lever rule in 2D via areas

(B) Common tangent construction

(C) Lever rule on each edge only

(D) Cannot be determined

58. In the Al–Si eutectic system, primary α (Al-rich) plates form in a hypoeutectic alloy. If cooling is too fast, primary α may:

(A) Fully transform to eutectic mixture

(B) Become dendritic instead of equiaxed

(C) Dissolve back into liquid

(D) Form martensite

59. The slope of the liquidus line in an isomorphic binary solid solution follows the Clapeyron relation. If ΔH_{fus} increases, the liquidus slope:

(A) Increases

(B) Decreases

(C) Unchanged

(D) Becomes negative

60. A peritectoid reaction ($\alpha + \beta \to \gamma$) occurs entirely in the solid state. Which system shows this?

(A) Fe–Fe_3C

(B) Cu–Ni

(C) Ni–Ti

(D) Ag–Pd

61. For a binary system with positive heats of mixing, the high-temperature phase diagram exhibits:

(A) Complete solubility at all T

(B) Miscibility gap at high T

(C) Monotectic reaction only

(D) Spinodal decomposition only

62. In a binary diagram, the eutectic microstructure's lamellar spacing λ scales with the growth rate V as:

$$\lambda^2 V = \text{constant}.$$

If V doubles, λ changes by factor:

(A) $1/\sqrt{2}$

(B) $1/2$

(C) $\sqrt{2}$

(D) 2

63. In the Fe–C system, pearlite forms by diffusion-controlled transformation along the TTT curve. The nose of the curve corresponds to:

(A) Maximum transformation rate

(B) Start of martensite formation

(C) Curie temperature

(D) Eutectic point

64. A metastable extension of the liquidus ("metastable eutectic") appears if kinetic inhibition prevents:

(A) Nucleation of the stable phase

(B) Diffusion in the solid

(C) Grain boundary migration

(D) Surface oxidation

65. The Gibbs–Thomson effect causes small precipitates to dissolve at temperatures higher than bulk equilibrium. As particle radius r decreases, the dissolution temperature:

(A) Increases

(B) Decreases

(C) Unchanged

(D) Oscillates

66. In a binary eutectic with limited solubility in solid phases, the lever rule fails near the eutectic because:

(A) Phase compositions vary with temperature

(B) Tie lines do not exist

(C) Diffusion is too fast

(D) Interface energies dominate

67. The "nose" of a TTT diagram corresponds to the minimum time for 50% transformation. For a given alloy, shifting the curve to longer times indicates:

(A) Faster kinetics

(B) Slower kinetics

(C) Same kinetics

(D) No transformation possible

68. Alloying with Mo in steel retards pearlite formation by:

(A) Lowering diffusion rates

(B) Raising hardenability

(C) Increasing Ms temperature

(D) Promoting bainite

69. Under continuous cooling (CCT) versus isothermal (TTT), the effective "nose" moves to:

(A) Longer times

(B) Shorter times

(C) Same time

(D) It disappears

70. What is the critical cooling rate to bypass pearlite formation estimated from the TTT by $T_{austentite} = 800°C$, $T_{nose} = 550°C$ after 10 seconds?

(A) 25°C/s

(B) 50°C/s

(C) 80°C/s

(D) 100°C/s

71. Bainite forms at temperatures below the pearlite nose but above Ms. Its morphology is controlled by:

(A) Shear plus diffusion

(B) Pure shear

(C) Pure diffusion

(D) Eutectic reaction

72. The incubation time for austenite -¿ pearlite at a given temperature is inversely proportional to:

(A) Nucleation rate

(B) Diffusion distance

(C) Grain size

(D) Ms temperature

73. In a TTT diagram, the start and finish curves for pearlite are separated because of:

(A) Finite growth rate

(B) Heterogeneous nucleation only

(C) Spinodal decomposition

(D) Martensitic transformation

74. A TTT curve for isothermal bainite shows two noses: upper bainite (UB) and lower bainite (LB). Which forms at lower temperature?

(A) UB

(B) LB

(C) They coincide

(D) Neither forms bainite

75. Jominy end-quench hardenability curves are analogous to CCT diagrams because they map:

(A) Cooling rate versus distance

(B) Composition versus hardness

(C) Time versus temperature

(D) Grain size versus hardness

76. Factors that shift the TTT nose to longer times include lower austenite grain size and:

(A) Higher C content

(B) Lower C content

(C) Higher Si content

(D) Lower Mn content

77. At temperatures just above Ms, the transformation to martensite upon quench is:

(A) Athermal (athermite)

(B) Isothermal

(C) Diffusion-controlled

(D) Nucleation-controlled

78. Continuous cooling transformation (CCT) diagrams differ from TTT by incorporating:

(A) Non-isothermal paths

(B) Higher accuracy only

(C) Alloy composition change

(D) Pressure effects

79. Total porosity ϕ_t and open porosity ϕ_o differ by:

$$\phi_o = \phi_t - \phi_{\text{closed}}.$$

Closed porosity does not contribute to:

(A) Fluid permeability

(B) Bulk density reduction

(C) Thermal insulation

(D) Acoustic damping

80. The Archimedes method for porosity uses immersion to determine:

(A) Open porosity only

(B) Closed porosity only

(C) Total porosity

(D) Pore size distribution

81. Mercury intrusion porosimetry measures pore throat sizes by relating pressure P to pore diameter d via Washburn:

$$P = -\frac{4\gamma \cos\theta}{d}.$$

Higher intrusion pressure corresponds to:

(A) Larger throats

(B) Smaller throats

(C) No pores

(D) Closed pores only

82. BET adsorption can estimate surface area and microporosity by fitting the isotherm to:

$$\frac{1}{V\left(P_0/P - 1\right)} = \frac{C-1}{V_m C}\frac{P}{P_0} + \frac{1}{V_m C}.$$

Here V_m yields:

(A) Monolayer volume

(B) Pore volume

(C) Total volume

(D) Closed porosity

83. In sintered ceramics, closed porosity reduces:

(A) Thermal conductivity

(B) Open-cell permeability

(C) Surface area

(D) Weight only

84. Permeability contrast between open and closed porosity is due to:

(A) Connectivity

(B) Pore size only

(C) Pore shape only

(D) Solid stiffness

85. Effective medium models (Maxwell–Garnett) for porosity predict composite elastic modulus reduction proportional to:

$$E_{\text{eff}} = E_0(1 - a\phi).$$

Open porosity $> 10\%$ yields $a \approx$

(A) 2–4

(B) 0.1

(C) 10

(D) 0.01

86. Differential pressure porosimetry uses increasing pressure steps to resolve:

(A) Pore size distribution

(B) Total porosity only

(C) Closed porosity only

(D) Density only

87. Image analysis of micrographs for porosity quantifies area fraction which equals volume fraction in:

(A) Isotropic microstructures

(B) Anisotropic microstructures

(C) Grained materials only

(D) Liquids only

88. Pore throat to body ratio influences:

(A) Relative permeability

(B) True density

(C) Closed porosity fraction

(D) BET surface area

89. Compaction of powders reduces porosity but may trap gas, leading to:

(A) Closed porosity

(B) Open porosity

(C) Zero porosity

(D) Increased permeability

90. Porosity anisotropy in extruded metals arises from:

(A) Directional pore alignment
(B) Chemical composition
(C) Grain boundary density
(D) Surface finish

91. The relationship between porosity and thermal conductivity in ceramics is:

(A) Inverse nearly linear
(B) Direct linear
(C) No relation
(D) Exponential

92. High-throughput porosity measurement by CT scanning relies on:

(A) X-ray attenuation contrast
(B) Mercury intrusion
(C) BET adsorption
(D) Archimedes method

93. Pore connectivity factor influences diffusion and is quantified by:

(A) Tortuosity
(B) Porosity only
(C) Contact angle
(D) Grain size

94. In pharmaceuticals, tablet disintegration time correlates with:

(A) Open porosity
(B) Closed porosity
(C) Grain size
(D) Particle shape

95. Freeze-drying introduces macroporosity by:

(A) Sublimation of frozen solvent
(B) Evaporation of liquid only
(C) Chemical etching
(D) Sintering

96. Porosity in polymer foams is typically achieved by:

(A) Gas blowing agents
(B) Mercury intrusion
(C) BET adsorption
(D) Archimedes immersion

97. In fuel cell electrodes, hierarchical porosity enhances:

(A) Mass transport

(B) Electrical conductivity only

(C) Thermal insulation

(D) Magnetic properties

98. Capillary pressure in porous media is inversely proportional to:

(A) Pore radius

(B) Tortuosity

(C) Solid density

(D) Viscosity

99. Porosity change during sintering follows:

(A) Exponential decay with time

(B) Linear decrease

(C) No change

(D) Oscillation

100. For a cubic crystal with $a = 4.00\,\text{Å}$ and Cu Kα radiation $\lambda = 1.54\,\text{Å}$, the (200) reflection appears at a Bragg angle $\theta \approx$

(A) 11°

(B) 22°

(C) 44°

(D) 68°

101. In the same cubic crystal ($a = 3.60\,\text{Å}$), the (111) peak is at $2\theta \approx 44°$ with Cu Kα. Using Mo Kα ($\lambda = 0.71\,\text{Å}$), the corresponding 2θ is nearest

(A) 21°

(B) 31°

(C) 44°

(D) 60°

102. A tetragonal cell has $a = b = 4.00\,\text{Å}$, $c = 5.00\,\text{Å}$. The ratio d_{002}/d_{200} is

(A) 0.80

(B) 1.00

(C) 1.25

(D) 1.50

103. A crystallographic plane intercepts the axes at $(\frac{1}{2}a, \infty, c)$. Its Miller indices (hkl) are

(A) (1 0 2)

(B) $(2\,0\,1)$

(C) $(0\,2\,1)$

(D) $(1\,2\,0)$

104. In a BCC lattice, which family is systematically absent?

(A) $\{100\}$

(B) $\{110\}$

(C) $\{200\}$

(D) $\{211\}$

105. In an FCC lattice, which reflection is allowed?

(A) (111)

(B) (210)

(C) (100)

(D) (310)

106. In reciprocal-space units, the radius of the Ewald sphere is

(A) $1/\lambda$

(B) $2\pi/\lambda$

(C) $\lambda/2$

(D) λ

107. In the CsCl structure, if $f_{\mathrm{Cs}} = f_{\mathrm{Cl}}$ exactly, which (hkl) would be extinct?

(A) (110)

(B) (200)

(C) (111)

(D) (002)

108. The strongest non-origin peak in a Patterson map corresponds to

(A) the self-vector at $(0, 0, 0)$

(B) the shortest interatomic vector

(C) the largest interatomic distance

(D) the average atomic position

109. In a Williamson–Hall plot of $\beta\cos\theta$ vs. $\sin\theta$, the intercept on the vertical axis yields information on

(A) microstrain

(B) crystallite size

(C) instrumental broadening

(D) lattice parameter

110. In space group $\mathrm{Pm\bar{3}m}$ (primitive cubic), which reflection is systematically absent?

(A) (100)

(B) (110)

(C) (111)

(D) none

111. Which plane family has the highest multiplicity in a cubic lattice?

(A) $\{100\}$

(B) $\{110\}$

(C) $\{111\}$

(D) $\{210\}$

112. At fixed θ, heavier elements scatter X-rays more strongly because their atomic scattering factor f

(A) drops off faster with angle

(B) has a larger magnitude

(C) is constant

(D) is purely imaginary

113. Hydrogen has a negative coherent neutron scattering length, which causes

(A) constructive interference

(B) destructive interference

(C) no contrast

(D) resonance scattering

114. The "phase problem" in crystallography refers to the inability to measure directly the

(A) structure-factor amplitudes

(B) structure-factor phases

(C) unit-cell dimensions

(D) Bragg angles

115. A key advantage of powder diffraction over single-crystal methods is that

(A) it requires no single crystal

(B) it gives directional intensities

(C) it solves phases directly

(D) it has no peak overlap

116. In a Debye–Scherrer camera of radius L, the ring radius R for a reflection at 2θ satisfies

(A) $R = L \sin 2\theta$

(B) $R = L \sin \theta$

(C) $R = L \tan 2\theta$

(D) $R = 2L\tan\theta$

117. A rocking-curve (ω-scan) width in single-crystal XRD primarily measures the crystal's

(A) lattice parameter

(B) mosaic spread

(C) thermal vibration amplitude

(D) unit-cell volume

118. The reciprocal-lattice metric for a hexagonal cell gives

$$\frac{1}{d^2} = \frac{4}{3}\frac{h^2 + hk + k^2}{a^2} + \frac{l^2}{c^2}.$$

For reflections with $l = 0$, which term dominates when $a \ll c$?

(A) the first (basal-plane) term

(B) the second (l-dependent) term

(C) both equally

(D) neither

119. For a hexagonal crystal with $a = 3.00\,\text{Å}$, the d-spacing of $(10\bar{1}0)$ is closest to

(A) $2.30\,\text{Å}$

(B) $2.60\,\text{Å}$

(C) $3.00\,\text{Å}$

(D) $3.50\,\text{Å}$

120. A real-space cell has volume $V = 100\,\text{Å}^3$. The reciprocal-cell volume V^* is

(A) $0.001\,\text{Å}^{-3}$

(B) $0.01\,\text{Å}^{-3}$

(C) $0.1\,\text{Å}^{-3}$

(D) $1\,\text{Å}^{-3}$

121. If $2W = 0.10$ in Debye–Waller theory, the diffracted intensity is reduced to approximately

(A) 90%

(B) 50%

(C) 10%

(D) 1%

122. A powder pattern with d-spacing ratios $1 : \frac{1}{\sqrt{2}} : \frac{1}{\sqrt{3}} : \cdots$ corresponds to which lattice?

(A) Simple cubic

(B) BCC

(C) FCC

(D) Tetragonal

123. In the diamond structure (space group $Fd\bar{3}m$), which reflection is forbidden?

(A) (111)

(B) (220)

(C) (200)

(D) (222)

124. In Laue diffraction, the condition $\mathbf{k} - \mathbf{k}_0 = \mathbf{G}$ implies that

(A) $|\mathbf{k}| = |\mathbf{k}_0|$

(B) $\mathbf{G} \perp \mathbf{k}_0$

(C) $\mathbf{k}$ is parallel to $\mathbf{k}_0$

(D) $\mathbf{G} = 0$

125. The Scherrer constant K depends on crystallite shape; for spherical crystals $K \approx$

(A) 0.5

(B) 0.9

(C) 1.5

(D) 2.0

126. In neutron diffraction, contrast between isotopes arises because

(A) different nuclear scattering lengths

(B) different atomic numbers

(C) different electron densities

(D) different magnetic moments only

127. Electron diffraction at 200 kV ($\lambda \approx 0.025\,\text{Å}$) yields nearly planar Ewald sphere, so zone-axis patterns show

(A) only one reflection

(B) many simultaneous reflections

(C) no reflections

(D) purely inelastic scattering

128. Kikuchi lines in TEM diffraction arise primarily from

(A) elastic Bragg scattering

(B) inelastic diffraction of thermal diffuse scattering

(C) fluorescent X-rays

(D) electron–electron scattering

129. The dynamical theory of electron diffraction predicts that

(A) forbidden reflections never appear

(B) intensities deviate from $|F|^2$

(C) λ depends on thickness

(D) phases are directly measured

130. Convergent-beam electron diffraction (CBED) patterns contain higher-order Laue zone (HOLZ) rings which can be used to determine

(A) lattice strain only

(B) absolute specimen thickness and symmetry

(C) only chemical composition

(D) only unit-cell volume

131. A crystal's mosaic spread will broaden Bragg peaks in

(A) powder Debye–Scherrer

(B) single-crystal rocking curves

(C) Laue back-reflection

(D) all of the above

132. The Debye scattering equation for total scattering (including diffuse) involves a sum over

(A) only Bragg peaks

(B) all interatomic pairs

(C) only nearest neighbors

(D) only unit-cell edges

133. The R factor in crystallographic refinement is defined as

(A) $\sum |F_{\mathrm{obs}} - F_{\mathrm{calc}}| / \sum F_{\mathrm{obs}}$

(B) $\sum |I_{\mathrm{obs}} - I_{\mathrm{calc}}| / \sum I_{\mathrm{obs}}$

(C) $\sum (F^2_{\mathrm{obs}} - F^2_{\mathrm{calc}}) / \sum F^2_{\mathrm{obs}}$

(D) all of the above (different conventions)

134. Systematic absences for a C-centred orthorhombic cell require $h + k =$

(A) even

(B) odd

(C) multiple of 3

(D) any integer

135. In electron diffraction, the extinction distance is the thickness over which

(A) a diffracted beam is completely extinguished by absorption

(B) primary and diffracted beams exchange intensity

(C) all reflections overlap

(D) only inelastic scattering occurs

136. A crystallographic twin law relates two domains by

(A) a rotation or reflection symmetry operation not in the point group

(B) a simple translation

(C) an arbitrary strain

(D) identical orientation

137. In powder indexing, the successively observed d-spacings of NaCl follow ratios $1 : \frac{1}{\sqrt{2}} : \frac{1}{\sqrt{3}} : \frac{1}{2} : \cdots$. The fifth observed peak corresponds to which (hkl)?

(A) (220)

(B) (200)

(C) (210)

(D) (211)

138. The ratio of integrated intensities I_{111}/I_{200} for an A1–type fcc crystal (one atom per lattice point) neglecting temperature and Lorentz factors is

(A) 1:1

(B) 2:1

(C) 3:2

(D) depends only on atomic form factor ratio $f(111)/f(200)$

139. In a reflection-geometry single-crystal experiment, the ω angle is the rotation about an axis

(A) perpendicular to the diffracting plane

(B) parallel to the incident beam

(C) through the detector

(D) none of the above

140. Anisotropic displacement parameters (ADPs) refine atomic vibrations as

(A) spherical shells

(B) ellipsoids

(C) rigid rotations

(D) constant offsets

141. The Patterson superposition method uses known heavy-atom positions to estimate

(A) light-atom positions

(B) unit-cell dimensions

(C) symmetry operators

(D) absorption coefficients

142. In a primitive orthorhombic cell, the number of symmetry-equivalent positions under point group mmm is

(A) 1

(B) 2

(C) 4

(D) 8

143. The Guinier approximation in small-angle X-ray scattering is valid for $qR_g < 1$, where $q = 4\pi \sin\theta/\lambda$ and R_g is the radius of gyration. It predicts $\ln I(q) \propto -q^2 R_g^2/3$. This allows direct extraction of

(A) crystal size

(B) particle shape

(C) radius of gyration

(D) lattice parameter

144. Relative density (specific gravity) compares the density of a material to that of water. A metal with relative density 7.8 has a density of approximately:

(A) 0.78 g/cm^3

(B) 7.8 g/cm^3

(C) 78 g/cm^3

(D) 0.078 g/cm^3

145. On the Mohs hardness scale, which mineral is harder than quartz (hardness 7)?

(A) Orthoclase feldspar

(B) Apatite

(C) Topaz

(D) Talc

146. The Rockwell hardness test measures indentation depth under a fixed load. A higher Rockwell number indicates:

(A) Greater indentation depth

(B) Smaller indentation depth

(C) Larger indenter diameter

(D) Lower applied load

147. Young's modulus is defined as the ratio of:

(A) Stress to strain in the elastic region

(B) Strain to stress in the plastic region

(C) Load to cross-sectional area

(D) Deflection to applied moment

148. Flexural strength (modulus of rupture) is determined from a three-point bend test by:

(A) Maximum tensile stress at fracture

(B) Maximum compressive stress at fracture

(C) Maximum shear stress at mid-span

(D) Average stress across the section

149. In a three-point bend specimen of rectangular cross-section, the flexural strength increases if:

(A) Span length increases

(B) Specimen thickness decreases

(C) Applied load at fracture increases

(D) Width decreases

150. Compressive strength is defined as the maximum compressive stress sustained before:

(A) Elastic limit

(B) Yielding

(C) Failure

(D) Necking

151. Fracture toughness K_{IC} characterizes a material's resistance to:

(A) Stable crack growth under mode I loading

(B) Plastic deformation at dislocations

(C) Surface hardness

(D) Creep at high temperature

152. A material with low fracture toughness is likely to exhibit:

(A) Ductile fracture

(B) Brittle fracture

(C) Superplasticity

(D) High fatigue life

153. Brittle fracture often occurs with little prior plastic deformation because:

(A) Crack tip blunting is extensive

(B) Energy is absorbed in dislocation motion

(C) Crack propagates rapidly without yielding

(D) Voids nucleate and coalesce first

154. Engineering stress is defined as load divided by the original cross-sectional area. True strain is defined as:

(A) $\Delta L/L_0$

(B) $\ln(L/L_0)$

(C) $(L - L_0)/L$

(D) $L/L_0 - 1$

155. In a tensile test, the linear elastic region ends at the:

(A) Ultimate tensile strength

(B) Yield strength

(C) Fracture point

(D) Proportional limit

156. For steel, Poisson's ratio is typically about:

(A) 0.1

(B) $0.^3$

(C) 0.5

(D) 1.0

157. The yield strength of a metal is defined at a specified offset, commonly:

(A) 0.01%

(B) 0.1%

(C) 1%

(D) 10%

158. Hardness correlates empirically with tensile strength because:

(A) Both measure resistance to elastic deflection

(B) Both involve plastic flow under load

(C) Both are independent of microstructure

(D) Both are measured on Vickers scale

159. A material shows 200 HV (Vickers hardness). Its approximate tensile strength is:

(A) 200 MPa

(B) 600 MPa

(C) 1000 MPa

(D) 2000 MPa

160. Creep is time-dependent deformation under constant stress. Primary creep exhibits:

(A) Increasing strain rate

(B) Decreasing strain rate

(C) Constant strain rate

(D) Rapid failure

161. Fatigue limit of steel refers to the stress amplitude below which:

(A) Plastic deformation accumulates

(B) No fatigue failure occurs

(C) Creep dominates

(D) Brittle fracture initiates

162. An Einstein solid with an Einstein temperature Θ_E has $C_V/R = 0.5$ at $T = \Theta_E$. What is the approximate value of C_V/R at $T = 2\Theta_E$?

(A) 0.6

(B) 1.0

(C) 2.0

(D) 2.5

163. Silver iodide undergoes an "order–disorder" transition with a sharp heat-capacity anomaly near its superionic transition at 420 K. This peak in C_p arises primarily from:

(A) Lattice vibrations only

(B) Electronic excitations

(C) Configurational entropy of Ag^+ mobility

(D) Magnetic ordering

164. In an ionic solid at room temperature, the dominant contribution to thermal conductivity is from phonons. Which mechanism most limits κ at high T ($T \gtrsim \Theta_D/2$)?

(A) Phonon–electron scattering

(B) Phonon–phonon Normal processes

(C) Phonon–phonon Umklapp processes

(D) Boundary scattering

165. Silicon has $\alpha = 2.6 \times 10^{-6}\,\mathrm{K}^{-1}$ at 300 K, while germanium has $\alpha = 6 \times 10^{-6}\,\mathrm{K}^{-1}$. This difference largely reflects:

(A) Mass difference only

(B) Bond anharmonicity differences

(C) Electronic contributions

(D) Gravitational effects

166. Garnet ($Y_3Al_5O_{12}$) has a low thermal expansion $\alpha \approx 5 \times 10^{-6}\,\mathrm{K}^{-1}$. Such low α in a complex oxide is due to:

(A) Strong covalent Al–O bonds

(B) Weak ionic Y–O bonds

(C) Magnetic ordering

(D) Porosity

167. In a metal at cryogenic temperature ($T \ll \Theta_D$), the electronic thermal conductivity κ_e dominates. According to the Wiedemann–Franz law $\kappa_e/\sigma T = L$, where L is the Lorenz number. A deviation from constant L indicates:

(A) Phonon drag on electrons

(B) Pure electron scattering

(C) Magnetic impurities only

(D) Perfect lattice

168. Diamond has $k \sim 2000$ W m^{-1} K^{-1}, $\rho = 3500$ kg/m^3, $c_p = 500$ J kg^{-1} K^{-1}. Its thermal diffusivity is roughly:

(A) 10^{-8} m^2/s

(B) 10^{-6} m^2/s

(C) 10^{-4} m^2/s

(D) 10^{-2} m^2/s

169. A polymer exhibits a jump in heat capacity at its glass transition T_g. This ΔC_p reflects increased segmental mobility. For a 100 g mol^{-1} polymer with $\Delta C_p = 0.5$ J g^{-1} K^{-1}, the molar jump is:

(A) 5 J mol^{-1} K^{-1}

(B) 50 J mol^{-1} K^{-1}

(C) 500 J mol^{-1} K^{-1}

(D) 5000 J mol^{-1} K^{-1}

170. In tungsten carbide (WC), the thermal expansion coefficient is $\alpha = 5 \times 10^{-6}\,\mathrm{K}^{-1}$, whereas for cobalt binder $\alpha = 13{\times}10^{-6}\,\mathrm{K}^{-1}$. Under rapid heating, this mismatch causes:

(A) Compressive stress in WC

(B) Tensile stress in WC

(C) No stress

(D) Shear failure only

171. Zirconium tungstate (ZrW_2O_8) exhibits isotropic negative thermal expansion over a broad temperature range. This counter-intuitive behavior is primarily due to:

(A) Rigid-unit transverse vibrations of WO_4 and ZrO_6 polyhedra

(B) Electronic delocalization upon heating

(C) Cation–anion size-mismatch strain relief

(D) Magnetostrictive domain reorientation

172. In diamond, the presence of the ^{13}C isotope (1.1 % natural abundance) introduces phonon scattering that limits its thermal conductivity. The scattering rate due to isotopic disorder scales with the mass variance $(\Delta M/M)^2$. This type of phonon scattering is known as:

(A) Mass-defect (isotope) scattering

(B) Phonon–electron scattering

(C) Phonon–phonon Umklapp scattering

(D) Grain-boundary (surface) scattering